Aircraft Winglet Design

Thesis · June 2020

DOI: 10.13140/RG.2.2.34449.92001

2 authors, including:

Hanlin Gongzhang
KTH Royal Institute of Technology
4 PUBLICATIONS **1** CITATION

SEE PROFILE

DEGREE PROJECT IN VEHICLE ENGINEERING,
SECOND CYCLE, 15 CREDITS
STOCKHOLM, *SWEDEN 2020*

Aircraft Winglet Design

Increasing the aerodynamic efficiency of a wing

HANLIN GONGZHANG

ERIC AXTELIUS

KTH ROYAL INSTITUTE OF TECHNOLOGY
SCHOOL OF ENGINEERING SCIENCES

Abstract

Aerodynamic drag can be decreased with respect to a wing's geometry, and wingtip devices, so called winglets, play a vital role in wing design. The focus has been laid on studying the lift and drag forces generated by merging various winglet designs with a constrained aircraft wing. By using computational fluid dynamic (CFD) simulations alongside wind tunnel testing of scaled down 3D-printed models, one can evaluate such forces and determine each respective winglet's contribution to the total lift and drag forces of the wing. At last, the efficiency of the wing was furtherly determined by evaluating its lift-to-drag ratios with the obtained lift and drag forces.

The result from this study showed that the overall efficiency of the wing varied depending on the winglet design, with some designs noticeable more efficient than others according to the CFD-simulations. The shark fin-alike winglet was overall the most efficient design, followed shortly by the famous blended design found in many mid-sized airliners. The worst performing designs were surprisingly the fenced and spiroid designs, which had efficiencies on par with the wing without winglet.

Content

Abstract 2

Introduction 4

Background 4

1.2 Purpose and structure of the thesis 4

1.3 Literature review 4

Method 9

2.1 Modelling the winglets 9

2.3 Flow computations 12

2.3.1 ANSYS Fluent 12

2.3.2 FloEFD - a Solid Edge plugin 14

Results 19

3.1 Modelled winglets 19

3.1.1 Split-tip designs 19

3.1.2 Blended design 19

3.1.3 Fenced design 20

3.1.4 Sharklet design 20

3.1.5 Spiroid design 21

3.2 CFD data 22

3.2.1 ANSYS Fluent 22

3.2.2 FloEFD 24

Discussion 26

4.1 Limitations and obstacles 26

4.2 Variance in CFD-results 26

4.3 CFD results versus Literature review 26

4.4 Trustworthiness of the CFD results 27

Conclusions 28

References 29

Introduction

1.1 Background

Due to the general acknowledgement of global warming, the aviation industry, along with many other transport industries, are faced with increasingly stricter emission regulations from government agencies around the world to reduce the carbon footprints of future aircraft. Thus, in today's world of aviation, winglets are primarily intended to increase the overall aerodynamic efficiency of aircrafts. They reduce the vortices generated alongside the surface of the wing by reducing the pressure gradient at the tip of the wing, hence equalizing the pressure difference between the upper and lower surface of the wing and minimizing the magnitude of the vortices generated during flight. This translates to decreased drag and better overall fuel economy without requiring any drastic modifications of an aircraft's structure elsewhere. However, various designs may offer different grades of performance depending on the physical dimensions, wing shape and flight characteristics of the aircraft. These aspects were the key reason behind the motive of conducting winglet studies for the X8 Skywalker.

The concept of attaching wingtip devices to the wing dates to the end of the 20th century. Several experiments and research were performed with few fixed-wing aircrafts, but it was not until the 1970s during the oil crisis that the idea got re-enlightened and commercialized among aircraft manufactures and aviation agencies.

Winglets, along with other wingtip devices can be considered a mainstream component among sub- and transonic modern aircrafts. They are seen in various aircraft sizes, ranging from small sized piston props to large jet propelled trans- and supersonic jets. Most of the winglets modelled in this project are based on the existing designs of today.

1.2 Purpose and structure of the thesis

The purpose of this thesis is to design an optimal winglet for the project's aircraft X8. The first goal is to determine the advantages and disadvantages of some existing winglet designs through literature review. The second goal is to replicate some of the most promising designs to date through CAD and thenceforth determine their efficiencies using CFD-simulations. Thus, a conclusion can be drawn regarding which of these designs are most suitable for the aircraft tasked to this project with given performance specifications.

1.3 Literature review

Online research has been carried out in order to find relevant information about various types of winglets and their characteristics. These include designs currently in-use alongside few state-of-the-art prototypes still being experimented. Information gathered was later summarized in this section. The sources include major aviation companies and agencies such as Airbus, Aviation Partners, Boeing, NASA and individual scientific papers written by experts within this field.

Figure 1: Whitcomb winglet on a KLM Royal Dutch Airlines' McDonnell Douglas MD-11

Richard T. Whitcomb was an American aeronautical engineer working for NACA (today NASA) that put extensive research into the area of winglets. In 1976 he introduced a new design consisting of one large upper plate and one smaller lower plate, as seen in figure 1 above. Whitcomb claimed that this design reduced the induced drag by about 20 percent and the wing-lift drag ratio of about 9 percent. This was done without increasing the bending moment in the wing fuselage compared to the wingtip device they compared with.[1]

Figure 2: Canted winglet on a South African Airways Boeing 747-400

The canted winglet was first introduced in the mid-80's by The Boeing Company, who aimed to extend the range and load capacity of its existing wide-body variants of 747-400 airliners and freighters. The resulting improvement turned out to be a 4% increase in the lift/drag-ratio. This was less than half of the upper limit of 9% suggested by the wind tunnel testing in the ACEE program, with much of the increase coming from the increased effective wing span.[2] However, the cant angle, or the angle between the plane of the winglet and the plane of the wing, cannot be decreased too much, as this affects the properties of the wing at higher angles of attack. With decreased cant angle, the flow separates more easily, and more intense vortices start to form at the tip section, reducing the efficiency of the winglet.[3]

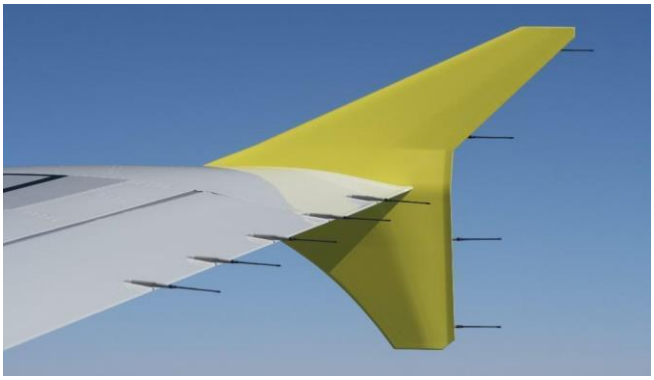

Figure 3: Fenced winglet of an Airbus A319-132

The “fence” design is Airbus’s answer to the canted winglets introduced by Boeing. It too was introduced in the mid 80’s aimed to decrease the overall fuel consumption of its aircraft. In contrast to the canted design, the winglets are cross sectionally double-sided and often perpendicularly attached to the wingtips, which results in a triangular, fence-looking winglet, hence earning its name as Wingtip fence.[4] The fenced winglet is often small compared to a other winglets, leading to a smaller reduction in the lift-induced drag at around 1.5-2% (at cruising conditions) compared to a wing without winglet. However, the smaller size results in a decreased bending moment in the fuselage.[5]

Figure 4: Split-tip winglet on a Boeing 737

The split-tip type winglet is an advanced type of winglet similar to the Whitcomb style due to its use of an upper and a lower plate, but with the difference in the size ratio between the two parts. It is used on the Boeing 737 MAX as seen in figure 4. Boeing calls their specific design 737 MAX AT (advanced technology) and it was announced in 2012.[6] The split-tip winglet may provide as much as 40 % improvement in cruising performance compared to existing blended designs, and a reduction in fuel burn by 1.5 % as well as a reduction of drag by up to 9.5 % compared to an unmodified wing.[7]

Figure 5: Blended winglet

The blended winglet consists of an upward swept extension of the wing. Compared to many other types, the blended winglet features a smooth chord transition instead of an angular transition from the wing to the winglet. Significant improvements of the lift/drag-ratio, up to almost 9%, can be seen even at very simple, non-optimized implementations of the design.[8] The design was initially investigated by Boeing in the mid-80s and further developed by Aviation Partners Inc in the early 90s. It was standard on Boeing Business Jet series but is also available on the 737-, 757- and 767-series. Boeing claims the use of blended winglets gives a decrease in fuel burn in the range of 4 to 5%.[9]

Figure 6: Shark fin-alike winglet on an Airbus A350 XWB

Having much resemblance with the blended winglets, the sharklets developed by Airbus also offer a smooth chord transition from wing to winglet. The design reminds of a shark fin, and hence the name sharklets. The sharklet was launched in 2013 as a retrofit to the Airbus A320 series with claims of a decrease in fuel burn up to 3.4%, resulting in a decrease of 700 tons of carbon emissions for each aircraft per year. The increased lift offered by the sharklets also provides a larger amount of cargo to be loaded.[10]

Figure 7: Split-scimitar winglet on a Boeing 737

Another type of winglet that also wears a lot of resemblance with the blended winglet is the split scimitar winglet, the name coming from its design reminding of two middle eastern style swords. It can be seen as a combination of a split tip wingtip but with the smooth chord transaction of a blended winglet. Optimized designs of the blended winglet have been compared to optimized designs of the split-scimitar winglet, where the latter provided a 4% decrease in drag and a 3% increase in lift.[11] Developed by Aviation Partners Inc and first put on test flight by United Airlines in 2013, the later company predicts this implementation will reduce fuel burn by 2 percent compared to previous designs, and save the company about 200 million dollars per year in fuel costs.[12] Using rough estimates, with a jet fuel price around 1,5 dollars per gallon (pre-Corona crisis), and 9,5 kg CO_2 produced from burning one gallon of jet fuel, that corresponds to around 1,3 million tons less CO_2 produced.

Figure 8: Raked wingtip on a Boeing 767-400

Not really a winglet but more of a wingtip device, the raked wingtip is a slightly swept-back extension of the wing, making the wing significantly longer than with the use of winglets. Raked wingtips fulfill the same purpose as winglets by improving the performance of the aircraft. Compared to a wing without winglet, a raked wingtip will increase the lift coefficient and reduce the drag coefficient in the range of 15-20% and 20-25% respectively (at an angle of attack of 8 degrees). Other benefits include a reduced noise level, reduced fuel burn and increased engine efficiency.[13] Some aircraft that have implemented this design are the Boeing 767, 777 and 787. On the 777-300ER (extended range), Boeing claims the use of raked wingtips will achieve a 2 percent lower fuel burn than previous designs, saving Boeing 140 000 dollars per year per plane.[14] With the same estimation as earlier, that corresponds to around 900 000 kg less CO_2 produced per plane.

Figure 9: Spiroid winglets on a Dassault Falcon 50

The spiroid type of winglets are, like the name suggests, a loop of a rigid ribbon. The design was first patented by Louis B. Gratzer in 1992, with claims of superior performance in reducing the lift induced drag.[15] If designed correctly, the effects of the wingtip vortices can be reduced significantly. Research has shown that the two vortex cores (formed due to low pressure regions at the bends of the spiroid), may combine into a single vortex. This single vortex follows a straight path behind the wing and does not cause negative interaction with the other parts of the fuselage, which in turns improves the range of the aircraft.[16] Spiroid winglets may also provide increased benefits at takeoff, as research has shown an increased lift coefficient at stall angles.[17] The design was first tested on the Gulfstream II in 1993, and later refined and tested on the Falcon 50 in 2010. Aviation Partners Inc are further investigating the design and technology for new implementation on a wide variety of jets.[18]

Method

2.1 Modelling the winglets

All winglet designs were carried out digitally by CAD-methodology. The choice of software was Solid Edge 2019, a widely used CAD software developed and provided by Siemens. The software was provided through KTH with an academic license.

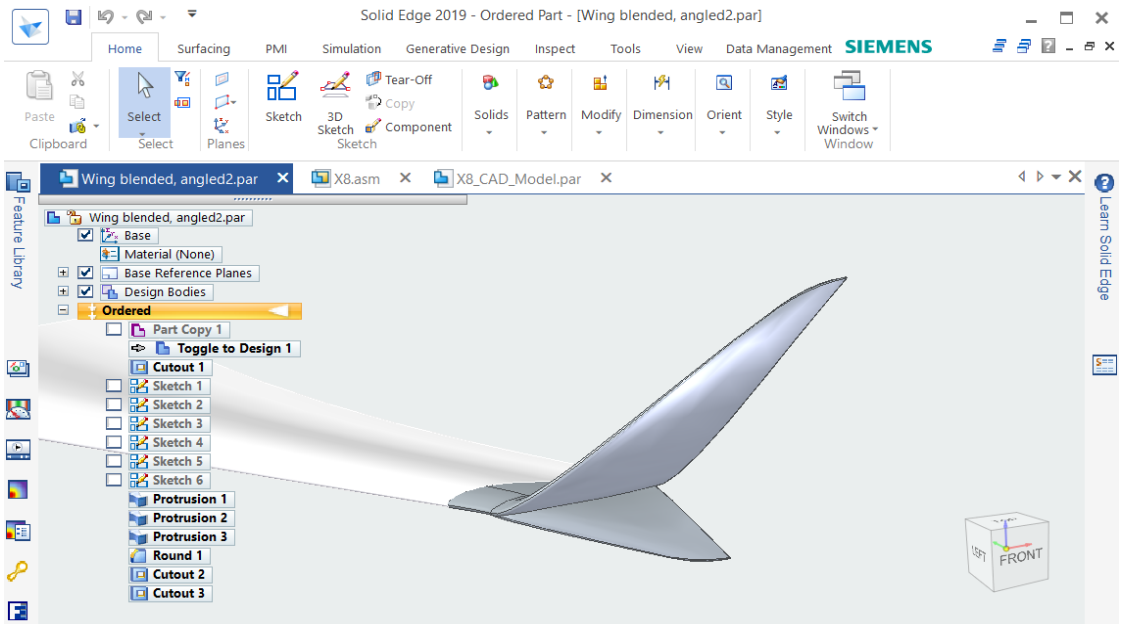

Figure 10: Solid Edge 2019 in par environment, designing a winglet.

The given 3D model of the aircraft is assembled by a total of six parts, with each wing being a separate part. Due to symmetry, all designs and CFD-simulations were performed on the left wing, hence excluding the remaining parts of the model assembly. The original model is show in figure 11.

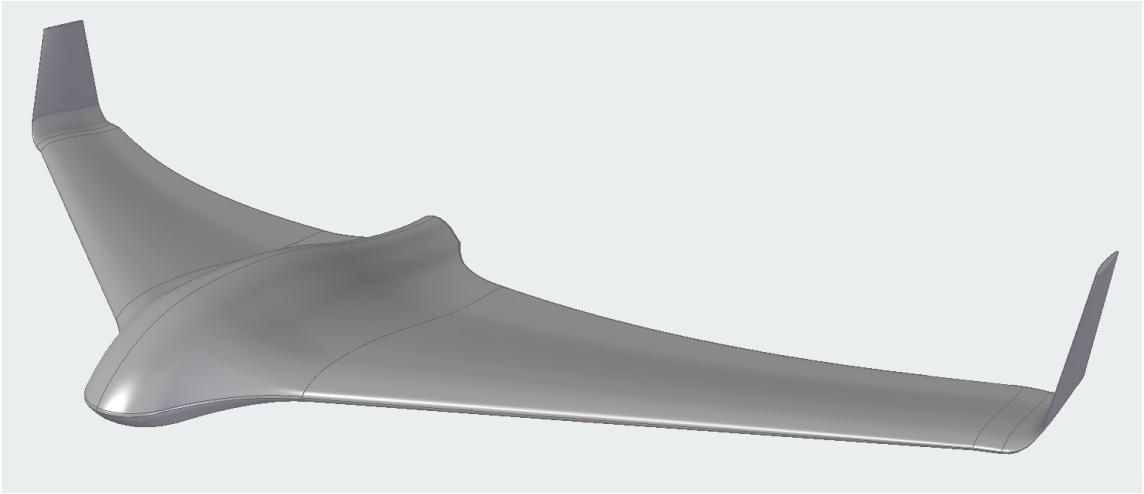

Figure 11: The X8 Skywalker

A new standard part was created in order to model various winglets to the x8. The original winglet was removed using the built-in cutout feature in Solid Edge, making room to protrude new solid features, as shown in figure 12 and 13.

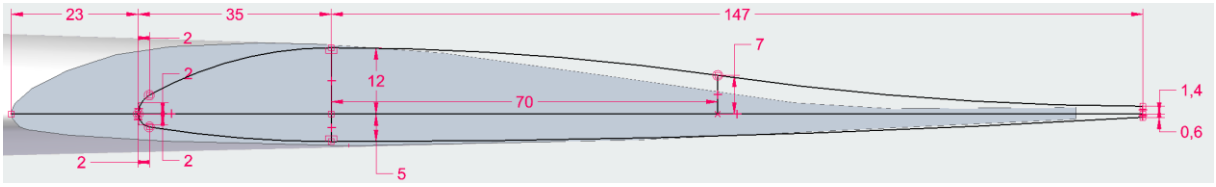

Figure 12: Defining the cross section (chord) of the wingtip, where the winglet's root is protruded from.

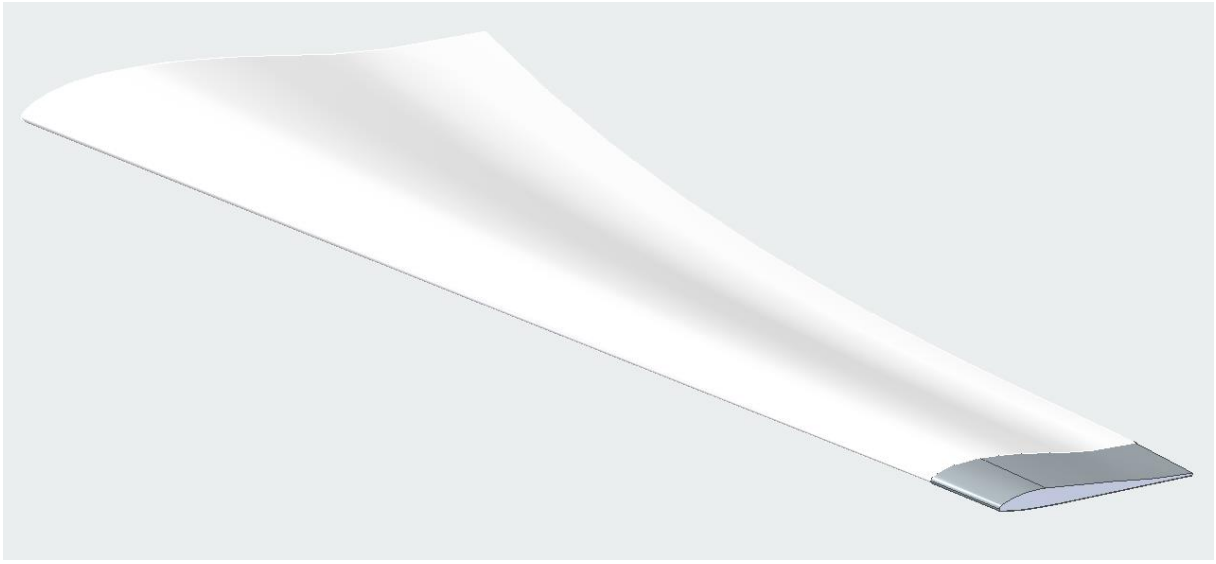

Figure 13: Summary view of the standard part, notice the protruded section (grey section), which is visualized in Figure 12.

A new constrained sketch, as shown in figure 5 and 6, was created along the lateral axis of the aircraft, where the sketches of the winglet's cross-section are guided through. This design approach offers the advantage of allowing the adjustments of the winglet's geometry with ease, eliminating the need of recreating a new part from scratch as long the modifications lays in the boundary of the winglet's type.

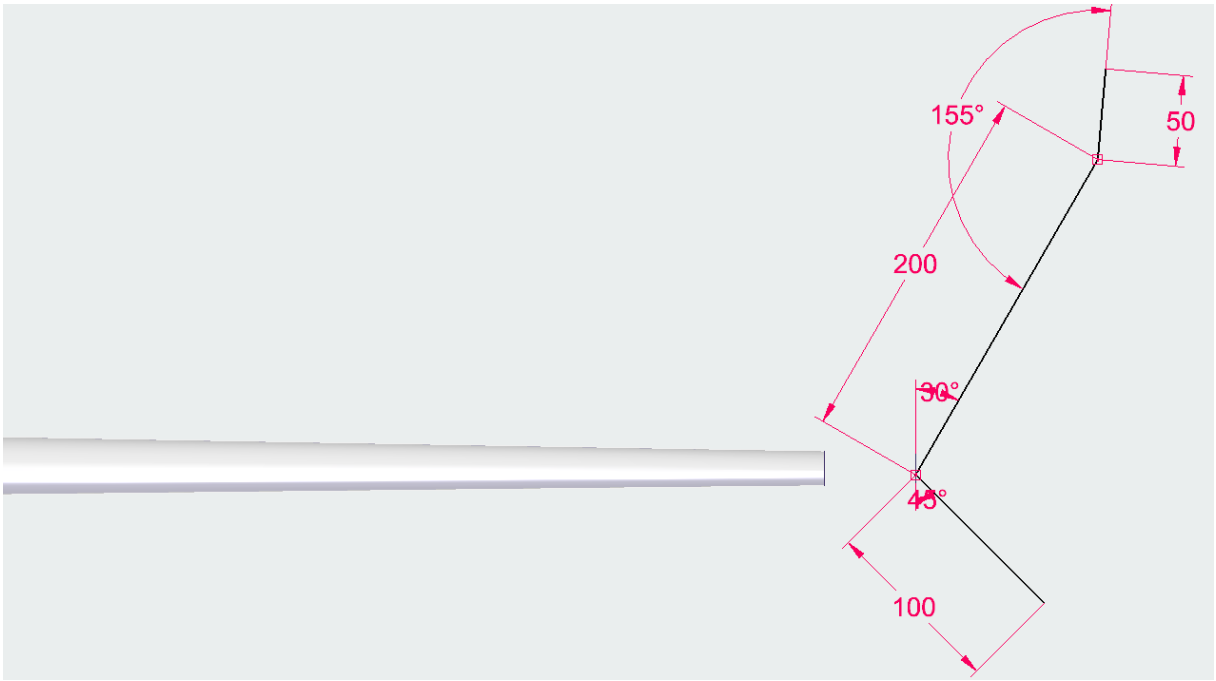

Figure 14: The guidelines in which the winglet's cross sections are guided through.

The guidelines in which the winglet's cross sections are guided through are show in figure 15 and 16. Each cross section is defined similarly to the main chord displayed in figure 12. Notice in figure 15 that the winglet's root is protruded normally from the wingtip's chord for a smooth geometric transition.

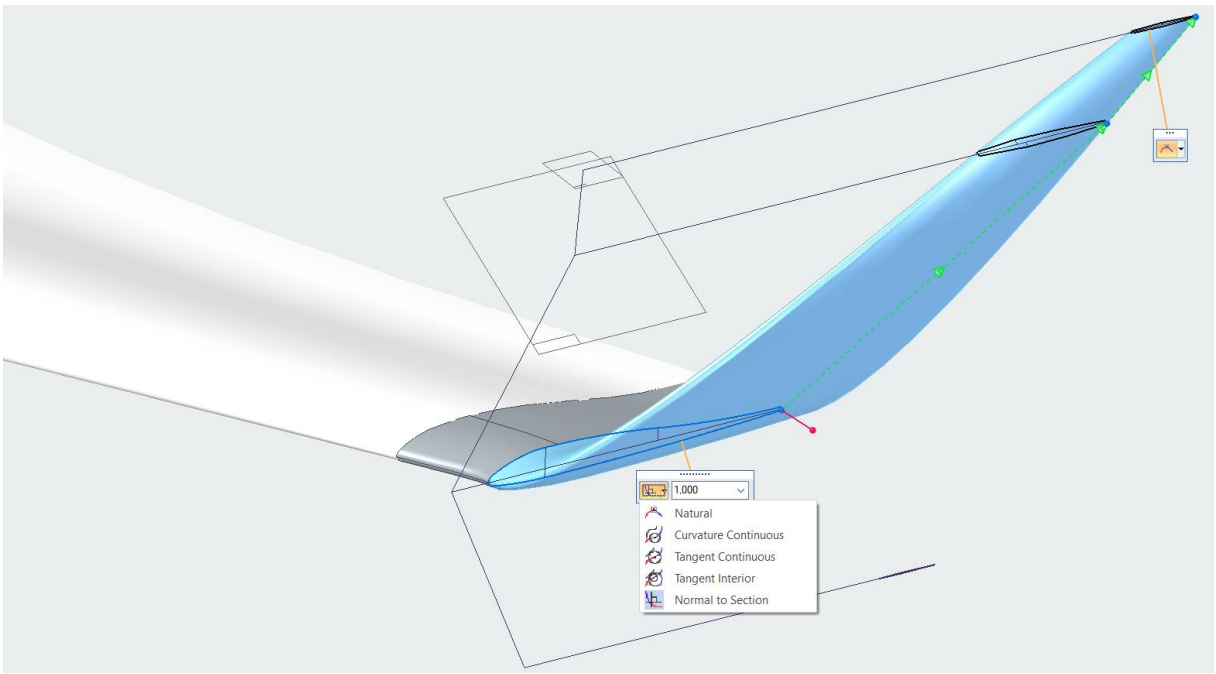

Figure 15: The protruded winglet with guided pathways.

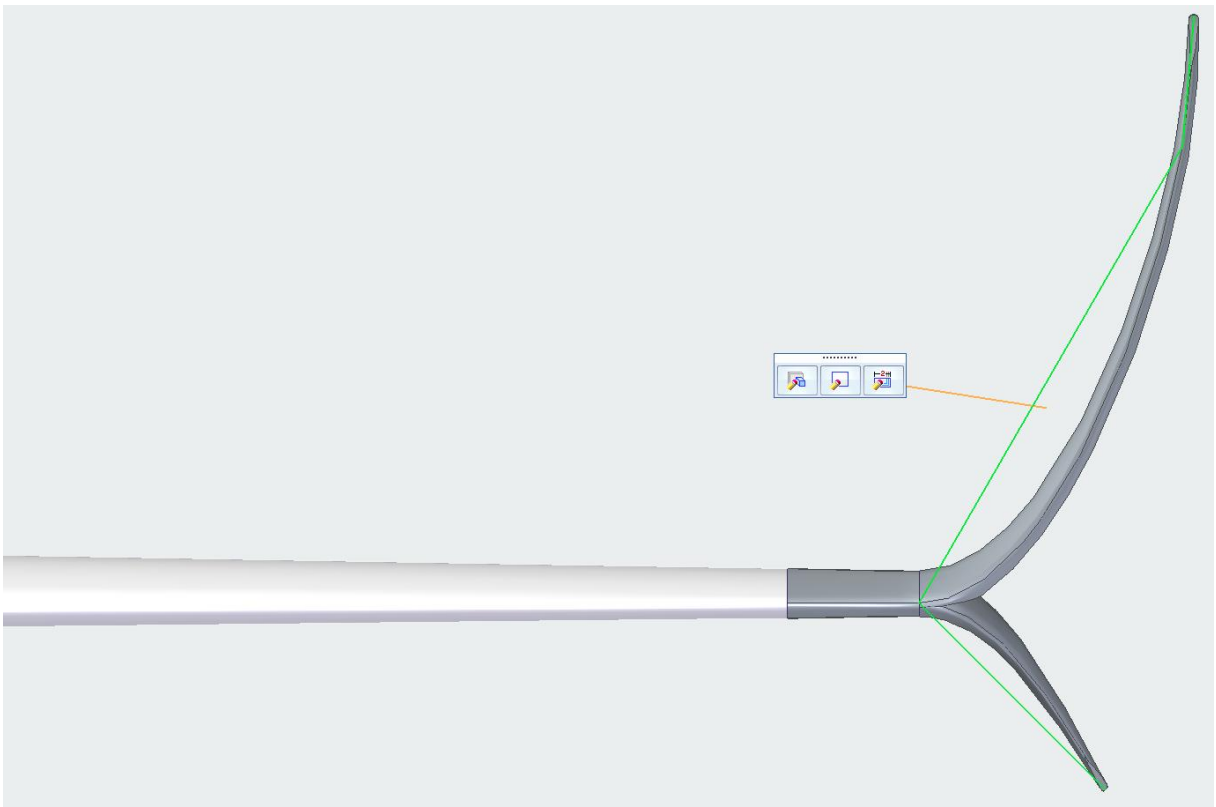

Figure 16: The guidelines from Figure 4 in front of the protruded winglet viewed from the front.

2.3 Flow computations

The lift and drag computations have been conducted in ANSYS Fluent 2019 R3 alongside FloEFD, which is a Solid Edge extension. Due to the limited knowledge and experience with CFD-software, simulations were performed parallelly with both software for result validation. This also increases the robustness and trustworthiness of the final results and the conclusions drawn from those.

The objective is to determine the lift and drag force generated when subjected to an incompressible flow speed of 100km/h (approximately 28m/s) under standard atmospheric pressure at 20°C for each respective design. The efficiency of the wing is thenceforth obtained by the ratio of the lift and drag forces of the wing as such:

$$\frac{L}{D} = \frac{C_l}{C_d}$$

Where C_l and C_d are the generated lift and drag coefficients of the wing.

2.3.1 ANSYS Fluent

ANSYS Fluent is an industrial computational software used for flow computations. It has a task-based workflow in which designing, meshing, solution and results are handled in separate sub-programs. The license to Ansys was provided by KTH, which only provides academic versions. Due to this, some features were limited, for instance a maximum limit of mesh cells/nodes of 512 000 is provided.

In Fluent, the workflow begins with designing or importing a geometry file into the DesignModeler. As all the models were designed in Solid Edge, the only required work in DesignModeler was to construct a computational domain (i.e. control volume) for the flow. This fluid domain is the volume surrounding the wing in which the airflow will be simulated. The dimension of the computational domain was set to (3,5 [x-axis] x 2 [y-axis] x 2 [z-axis] m; length x width x height). The wing has been centered in the z- and y-axis but its center is 1,5 m from the front wall on the x-axis. All the models were tested at angles of attack 2, 4, 6, 8 and 10 degrees with respect to the incoming flow. The xyz-system, as well as the wing in the control volume, is illustrated in figure 17.

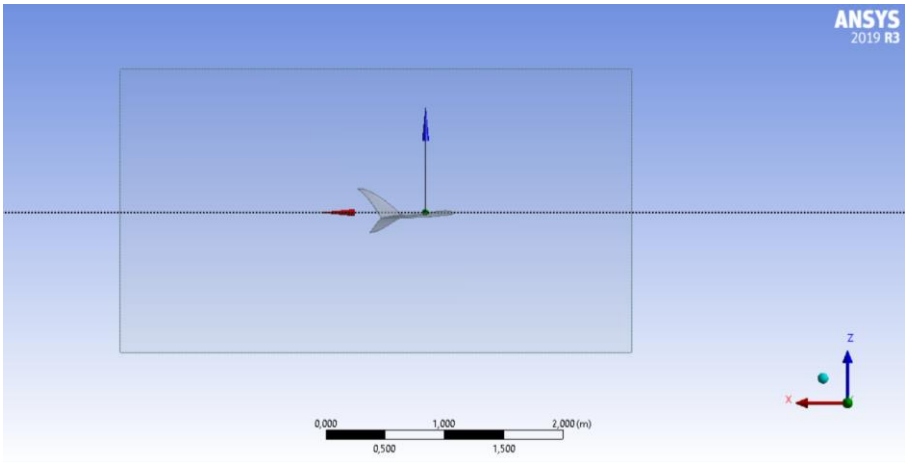

Figure 17: Control volume and coordinate system in DesignModeller

The selected geometry was then preprocessed in Meshing, Ansys' mesh-generating program. The meshing was done mostly with the preset settings (creating an unstructured grid with pyramid and tetrahedra elements), except for the maximum element size that was set to around 0,25 m. Some models had a slightly more complex geometry, which required more elements and nodes in the mesh. In that case, the maximum element size had to be slightly larger to allow for the limit of 512 000 elements/nodes not to be exceeded. Another exception was a slightly larger maximum element size at the borders of the control volume, an area with less interest. This allowed for more cells in the area around the wing. More cells typically translate to more precise results, but at a cost of increased computation time, and in the case of this project also means exceeding the academic license limit of 512 000 elements. A cross section (xz-plane) of the meshed control volume and wing seen in figure 1 is shown in figure 18. The region with very fine mesh is where the wing is positioned, and as can be seen the element size grows while approaching the borders.

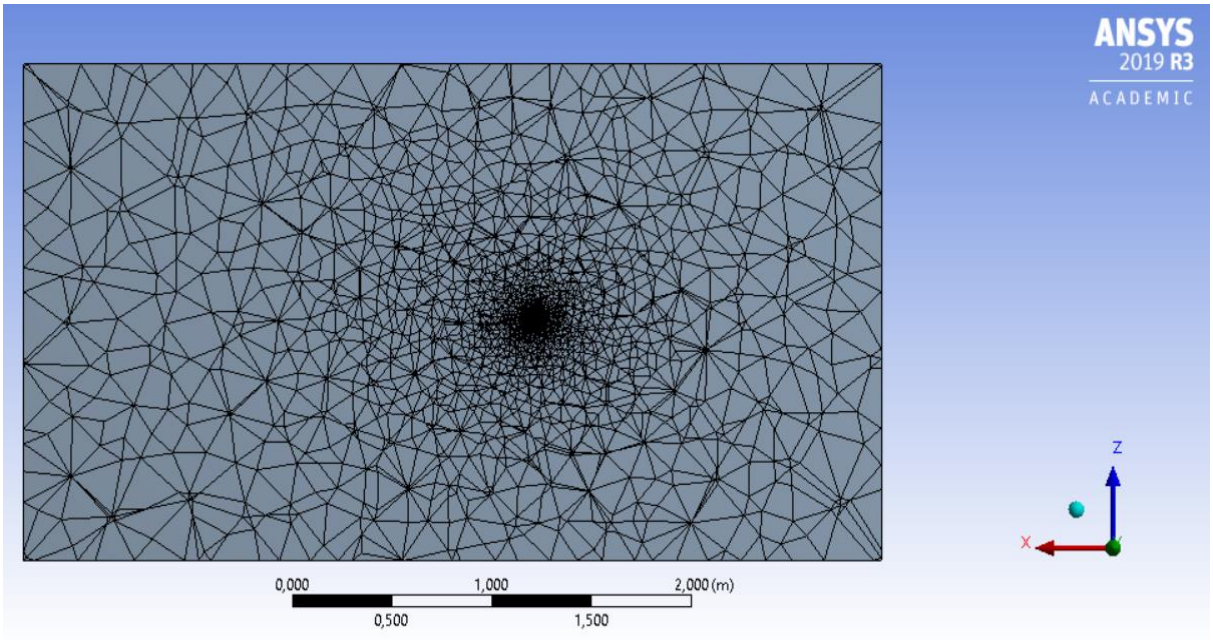

Figure 18: Meshed control volume and wing

The solver can be configured in the program setup when the mesh is ready. The setup consists of choosing a model, solving method, boundary conditions, and number of computation iterations. The boundary conditions consisted of a velocity inlet at 28 m/s (approx. 100 km/h, or Mach 0,08) with direction in the x-axis, a pressure outlet facing the velocity inlet, and walls at the remaining surfaces. The walls were modeled with standard wall functions, which is commonly used when modelling industrial flows.[19] To simulate viscous flow, no-slip condition was used on all surfaces (default setting in Fluent).

As turbulence model, the pressure based standard K-epsilon was chosen. Here, the pressure based setting means that the flow is incompressible (justified by the Mach number being lower than 0,3), and the standard K-epsilon model consists of 2 transport equations (PDE:s) with two variables, namely turbulent kinetic energy and turbulent dissipation. Little was known about turbulence modelling beforehand, so the decision on what turbulence model to use was decided by the fact that the K-epsilon model is well known and widely used.[20] It is commonly used for external flows with complex geometries, but also serves a good general purpose model that is not memory-intense on the computer and offers good convergence.[21] To solve the PDE: s, second order upwind schemes were used. These upwind

schemes take values upstream to calculate the values of the mesh cells downstream. The second order schemes use two points upstream compared to one point used by the first order schemes, which provided better accuracy but made it more difficult to converge. When the solver was initiated, physical properties chosen to compute are reported for each iteration. The solver was set to 100 iterations, which gave enough time for the solution to converge.
When the solver is done, post-analysis is provided in the program Results. From here, information about pressure, velocity, streamlines, etc. can be retrieved. An example of this is shown in figure 19.

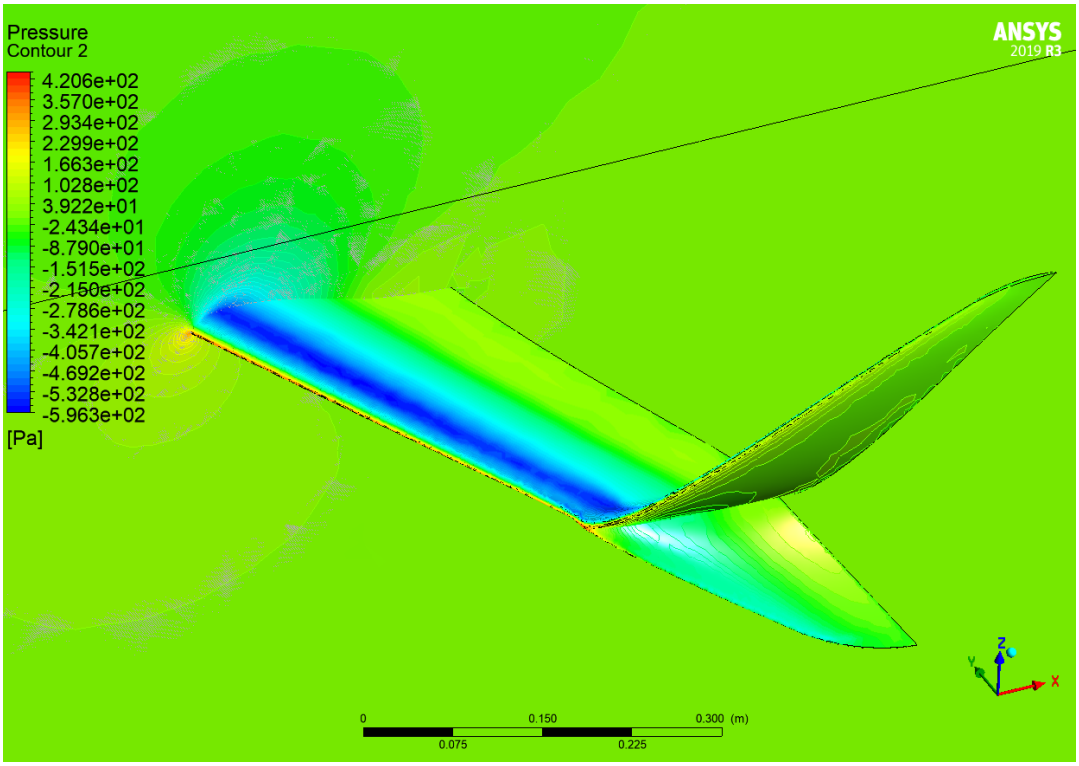

Figure 19: Contour map of pressure difference after a simulation

2.3.2 FloEFD - a Solid Edge plugin

Developed by Mentor, as part of the Siemens group, FloEFD is available as an extension for Solid Edge and many CAD software. It provides a relatively simple interface with straightforward steps to quickly perform various types of CFD-simulations, both for external and internal flow. The software plugin is available as an academic version for Solid Edge, with the compromise of watermarks displaying over the computational domain during simulations. The academic license can be obtained upon request at Mentor's website.

Since FloEFD is offered as a plugin for Solid Edge, all designed parts can be directly analyzed within the assembly environment in Solid Edge without the need of importing any 3D part.

The workflow begins with creating a project by defining the necessary flow conditions and desired boundary conditions for the computational domain. The flow analysis consists only of the wing's external surface, and heat conduction and other similar physical processes were neglected since they are irrelevant when studying incompressible flow conditions. The configuration settings for the desired flow condition are shown in figure 21.

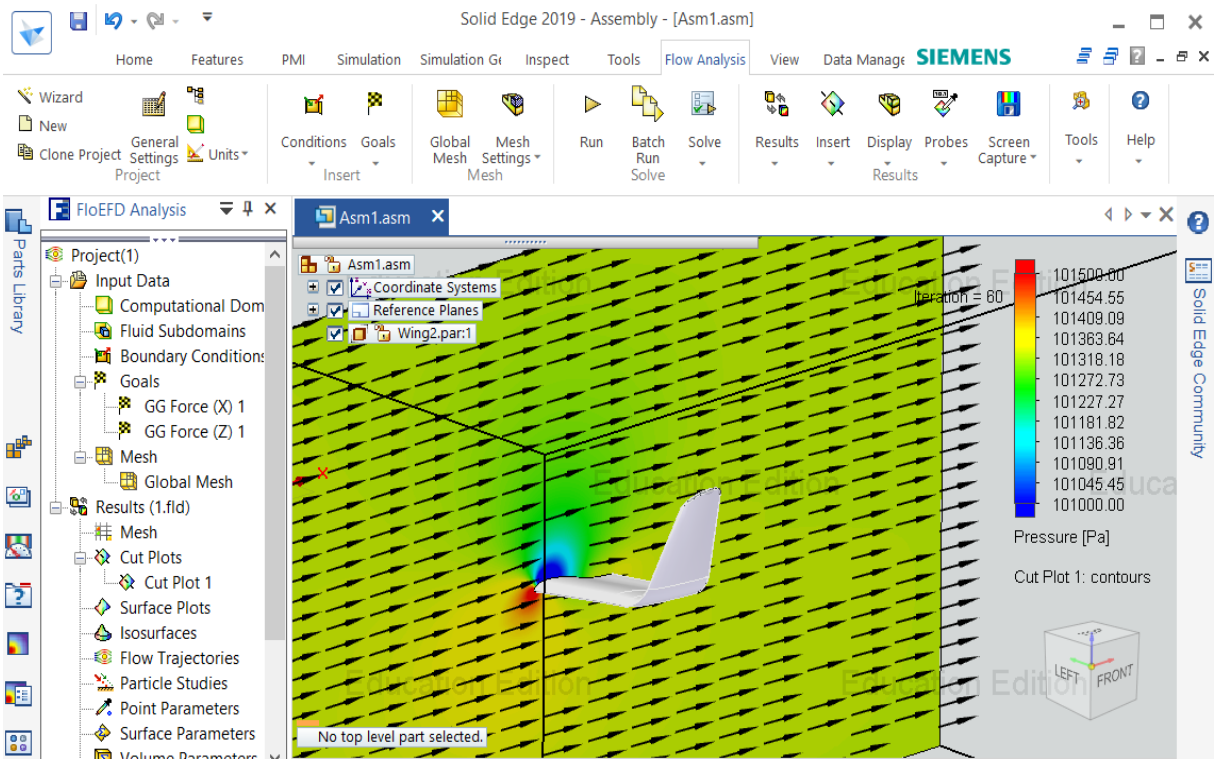

Figure 20: FloEFD interface, showing cross section pressure gradient of the wing.

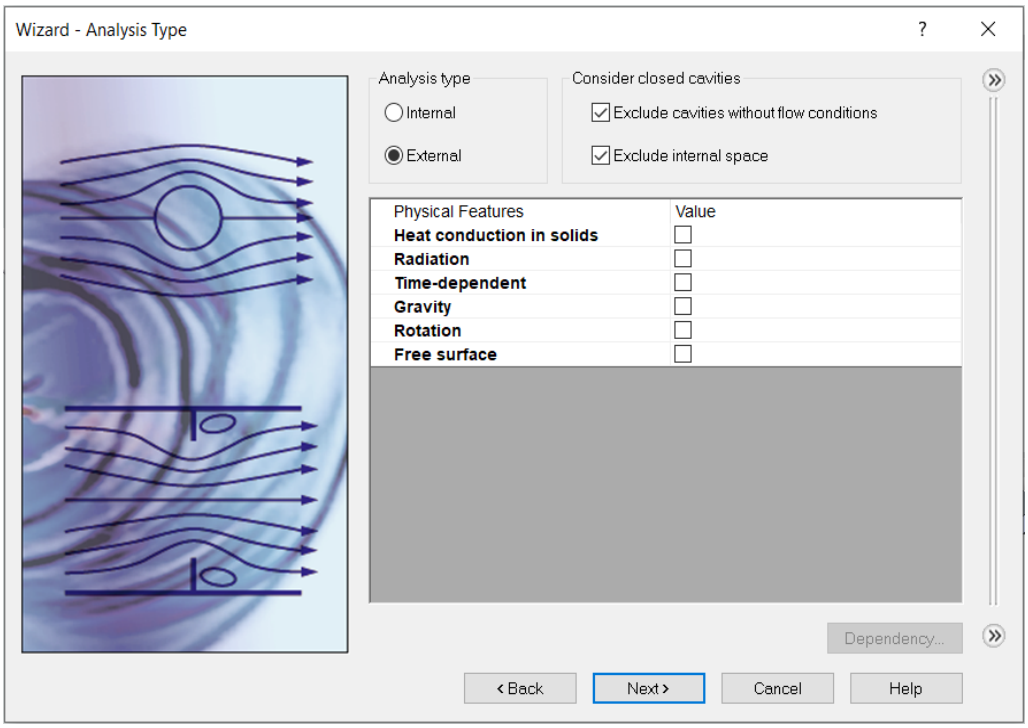

Figure 21: Configuring analysis type and physical features

The choice of fluid was air, with high Mach number flow and humidity criteria neglected since low-speed flows are generally considered isochoric (i.e. incompressible). The fluid configurations are displayed in figure 22. Finally, the pressure, temperature and flow velocity were set to the specified values mentioned in section 2.3, and the direction of flow was set along the longitudinal direction of the aircraft (x-axis). The initial and ambient condition configurations are shown in figure 23.

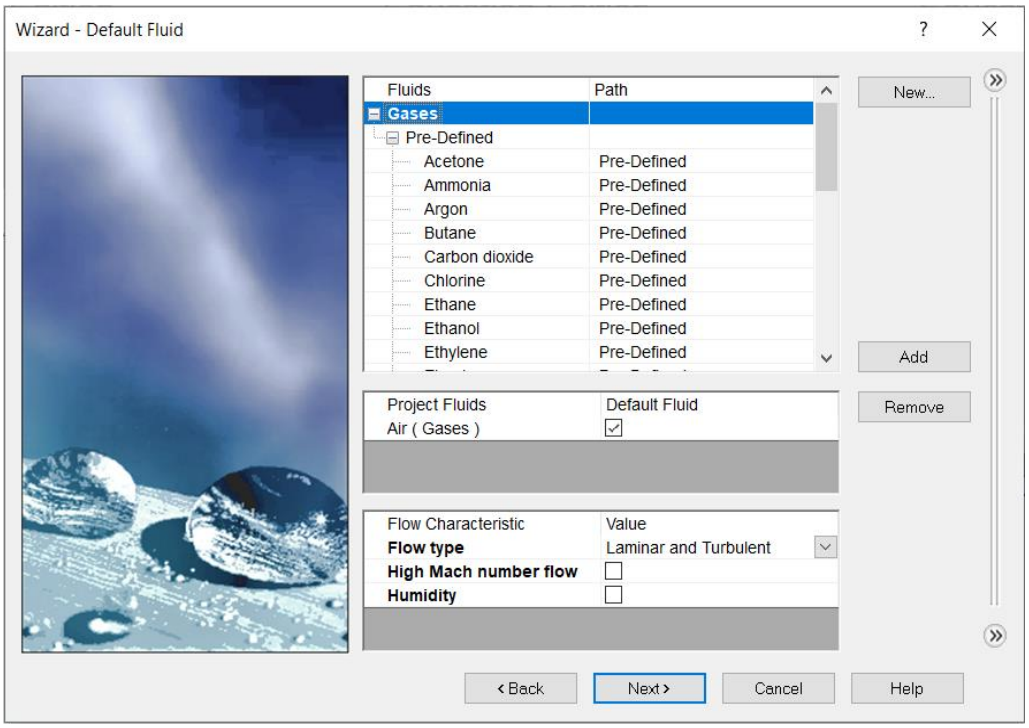

Figure 22: Selecting fluid medium and its flow characteristics

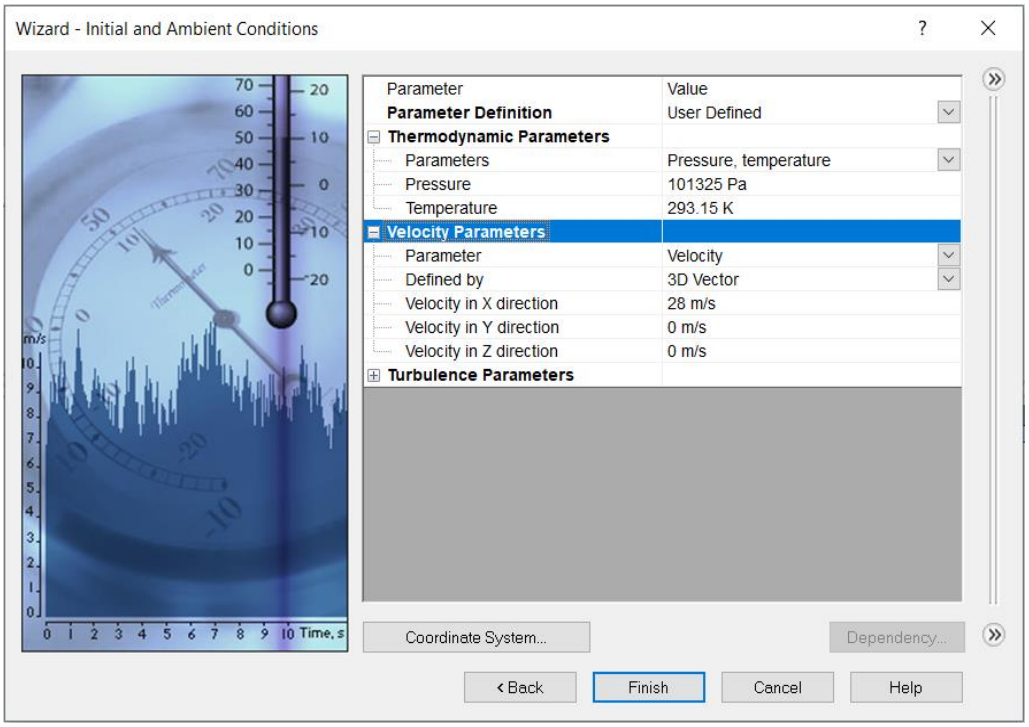

Figure 23: Configuring the direction of flow and streaming velocity.

The dimension of the computational domain was set to (2 [x-axis] x 1.5 [y-axis] x 1 [z-axis] m^3; length x width x height), which was marginally smaller than the domain in ANSYS Fluent. Here, the trailing edge (x/L = 1) of the root chord is centered at the origin of the coordinate system. The computational domain is consisted of uniformed mesh grids with a grid size of 0.01 x 0.01 x 0.01 m^3, giving a total of 3 000 000 elements, as shown in figure 24. The computational domain is consisted of uniformed mesh grids with a grid size of 0.01 x 0.01 x 0.01 m^3, giving a total of 3 000 000 elements, as shown in figure 25.

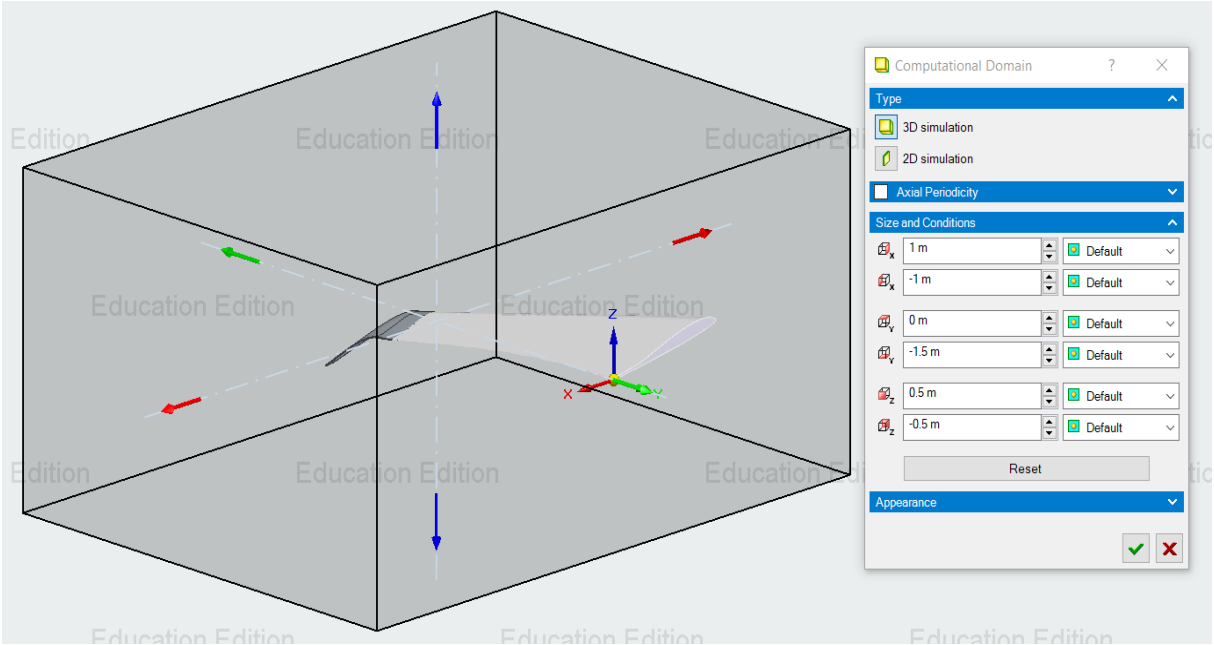

Figure 24: Dimensioning the computational domain, with the left cross-section of the wing not offsetting the domain's left wall.

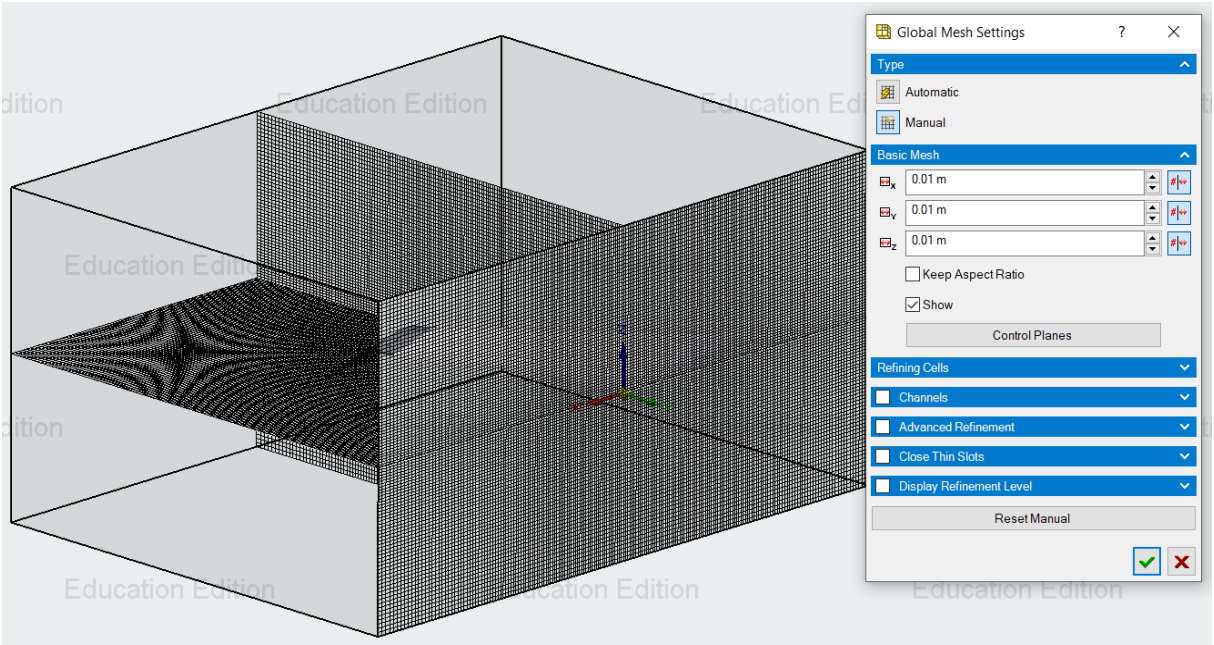

Figure 25: Configuring mesh settings.

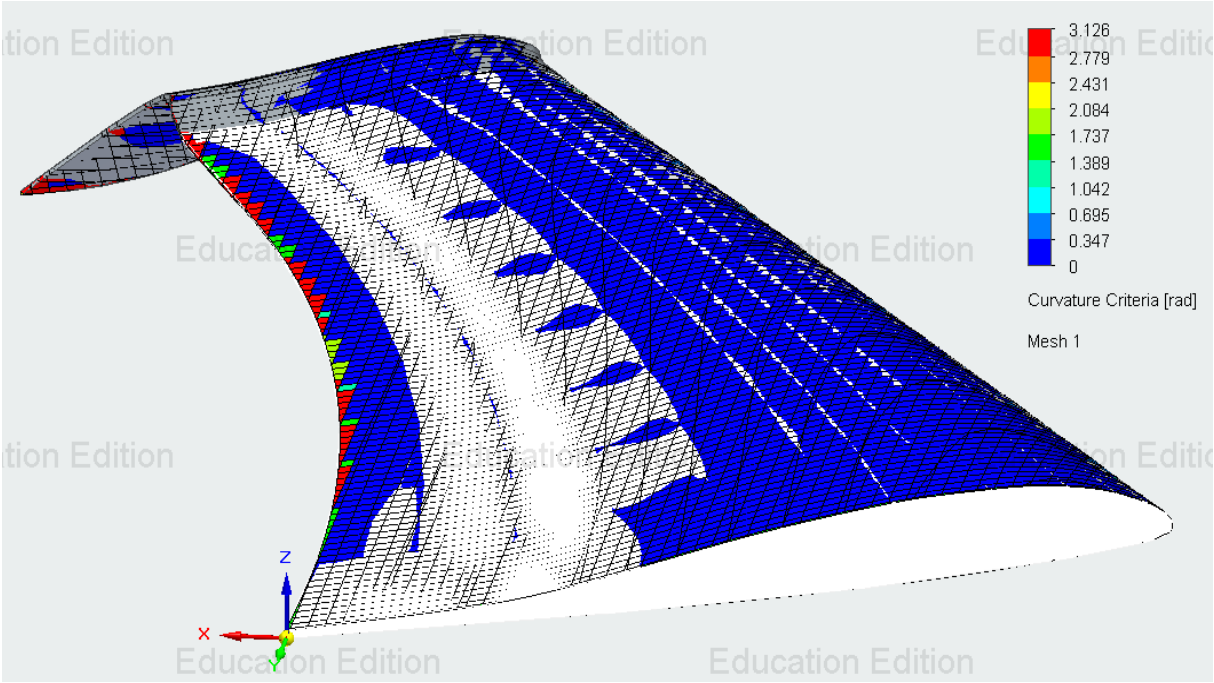

Figure 26: Mesh of the wing.

The curvature criteria of the wing body are shown in figure 26. Sections with warmer mesh grids are more refined to cooler regions since these grids girt more complex geometries. These regions require therefore more computational time to mesh and simulate compared to the cooler grids. Each grid can be considered as a subdomain of the global domain shown in figure 24 and 25, meaning that the global results are the sum of the local results evaluated from respective subdomain.

Results

3.1 Modelled winglets

The final designs are listed in the following subsection, with 5 unique variants. The split-tip and sharklet design both contain two derivatives, making a total of 7 winglets. The images were rendered by KeyShot 7, a CAD rendering which was included in the Solid Edge 2019 under academic license.

3.1.1 Split-tip designs

The two variants of the split-tip design inspired from Boeing's latest 737 derivatives are shown in figure 27. The variant to the left of figure 27 shares the shapes characteristics of an ordinary blended winglet whereas the one to the right features a smooth geometrical transition throughout the winglet.

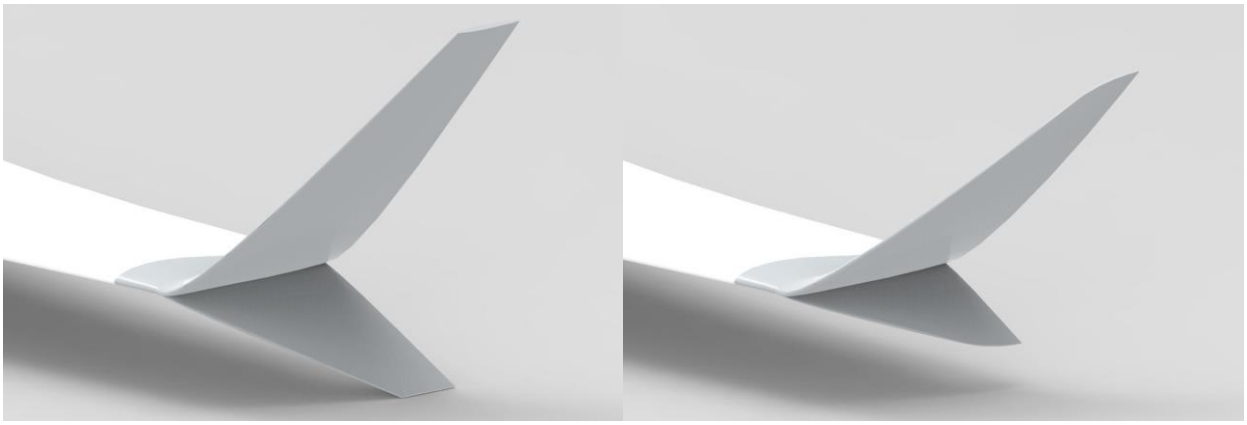

Figure 27: Split-tip winglets

3.1.2 Blended design

Blended winglets can be found in many existing mid-sized Boeing jetliners. In contrast to those, the blended design modelled in this project features an elliptical shape, which is shown in figure 28. It can be of interest to compare this design with the original winglet of X8, which is an ordinary blended design.

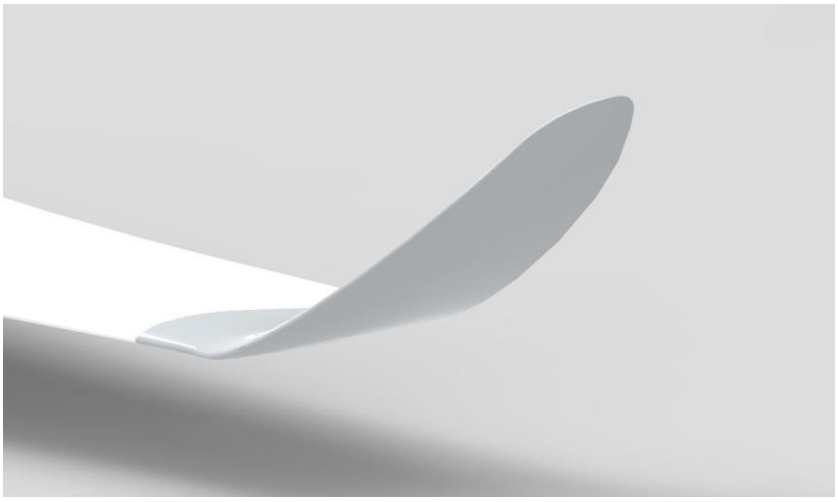

Figure 28: Blended winglet

3.1.3 Fenced design

The fenced design similarly to those used on older Airbus aircrafts is shown in figure 29. This was the easiest winglet to model since there are no smooth transition between the wingtip and the winglet, and probably the easiest to manufacture and install.

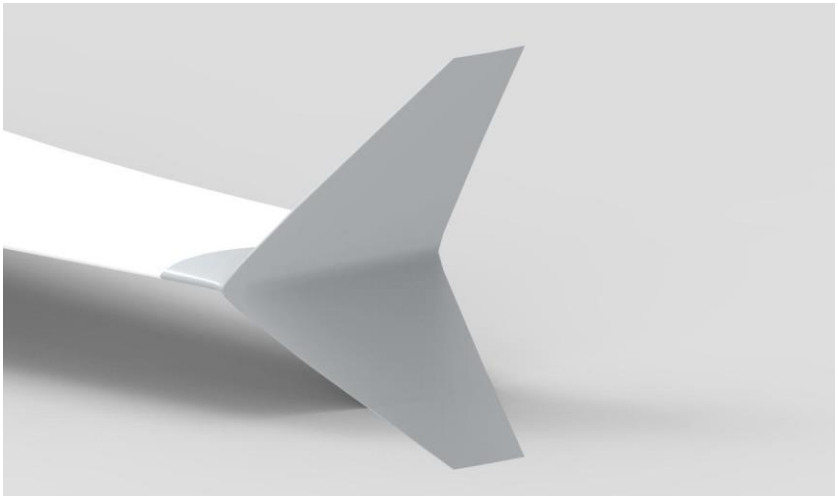

Figure 29: Fenced winglet

3.1.4 Sharklet design

The sharklet design similarly to those found in more recently manufactured Airbus jetliners and smaller piston powered light aircrafts are shown in figure 30. The variant to the left has its tip faced upwards while the one to the right is faced towards the ground.

Figure 30: Sharklet

3.1.5 Spiroid design

The spiroid design is shown in figure 31. This was the most challenging winglet to model due to its complex geometry. A pathway with serval cross-section sketches were created to guide the protruded feature throughout the spiral.

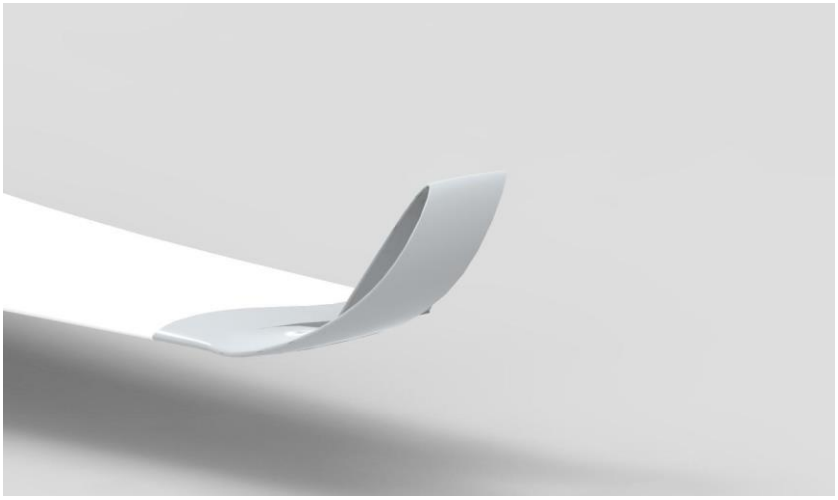

Figure 31: Spiroid

3.2 CFD data

3.2.1 ANSYS Fluent

The lift, drag and Lift/Drag-ratio obtained from computations in Ansys Fluent is presented in table 1. In figure 32, the same data is presented graphically, where alpha denotes the angle of attack.

Table 1: Lift, drag and Lift/Drag-ratio obtained from computations in Fluent.

Design	Force [N]	α = 2	α = 4	α = 6	α = 8	α = 10
Without winglet	Lift	9,36	22,69	36,6	50,06	64,76
	Drag	2	2,33	3,1	4,37	6,11
	L/D	4,68	9,74	11,81	11,46	10,59
Original (unmodified)	Lift	12,95	26,42	40,82	54,24	68,45
	Drag	2	2,42	3,3	4,62	6,38
	L/D	6,48	10,92	12,37	11,74	10,73
Split-tip	Lift	14,69	28,71	44,34	59,82	74,34
	Drag	2,27	2,71	3,61	5,02	6,95
	L/D	6,47	10,59	12,28	11,91	10,7
Split-tip sharklets	Lift	12,71	27,58	42,47	56,78	70,97
	Drag	2,11	2,57	3,45	4,86	6,74
	L/D	6,02	10,73	12,31	11,68	10,53
Blended	Lift	14,01	28,64	43,34	58,42	72,86
	Drag	2,12	2,58	3,45	4,84	6,61
	L/D	6,61	11,1	12,56	12,07	11,02
Fenced	Lift	12,91	26,7	40,09	55,86	68,84
	Drag	2,13	2,57	3,39	4,82	6,49
	L/D	6,06	10,4	11,83	11,59	10,61
Sharklets, upwards	Lift	13,92	28,3	43,66	58,67	73,24
	Drag	2,03	2,48	3,42	4,87	6,72
	L/D	6,86	11,41	12,76	12,04	10,9
Sharklets, downwards	Lift	13,2	27,82	42,7	57,75	71,47
	Drag	1,97	2,45	3,37	4,82	6,63
	L/D	6,7	11,36	12,67	11,98	10,78
Spiroid	Lift	13,21	27,73	42,07	56,61	70,86
	Drag	2,23	2,66	3,56	4,9	6,89
	L/D	5,92	10,42	11,82	11,55	10,28

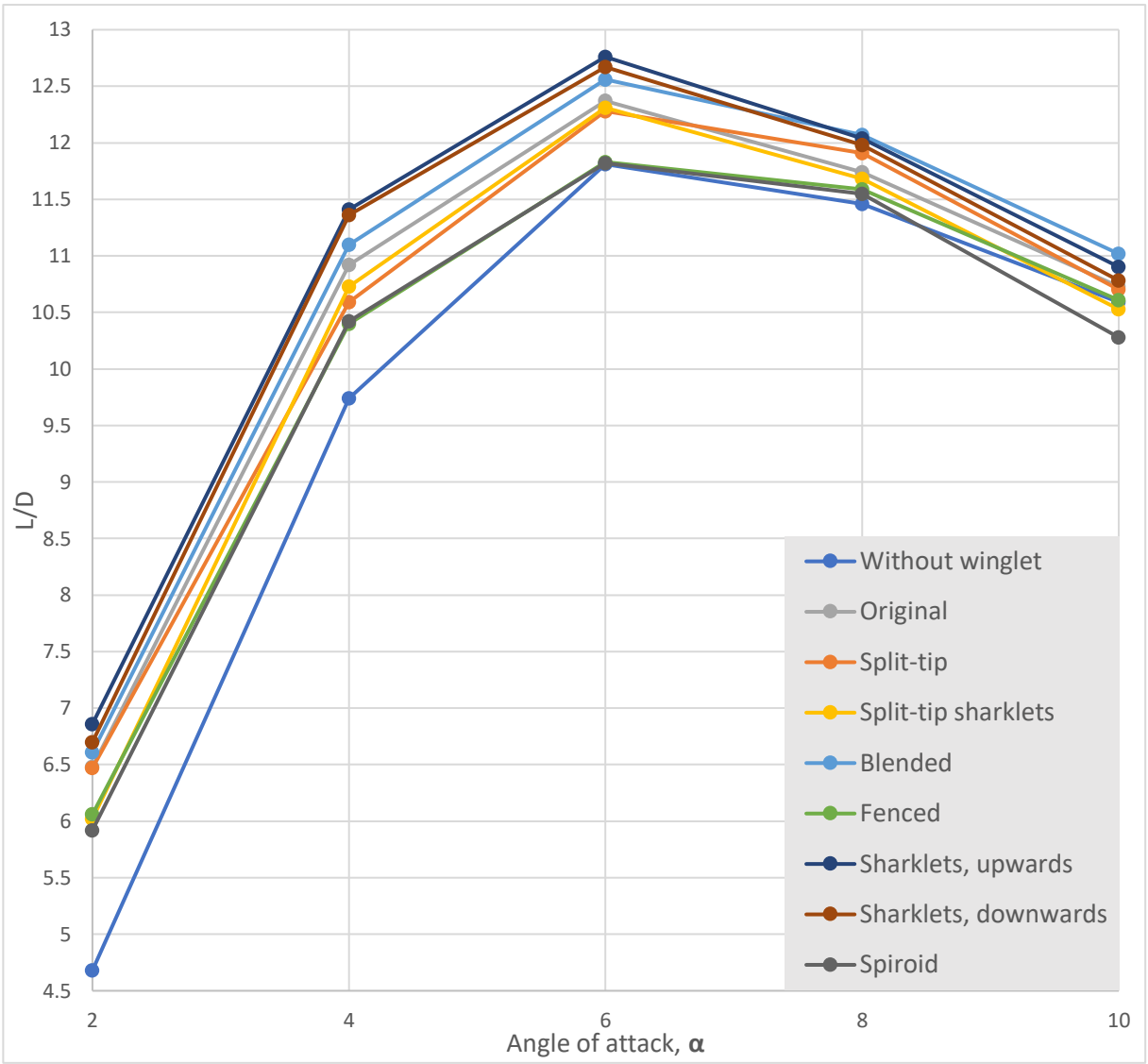

Figure 32: the angle of attack versus the Lift/Drag-ratio evaluated from ANSYS Fluent

3.2.2 FloEFD

The lift, drag and Lift/Drag-ratio obtained from computations in FloEFD is presented in table 2. In figure 33, the same data is presented graphically, where alpha denotes the angle of attack.

Table 2: Lift, drag and Lift/Drag-ratio obtained from computations in FloEFD.

Design	Force [N]	α = 2	α = 4	α = 6	α = 8	α = 10
Without winglet	Lift	9,82	19,09	28,08	36,70	43,47
	Drag	1,96	2,30	3,24	4,53	6,17
	L/D	5,00	8,30	8,66	8,11	7,04
Original (unmodified)	Lift	10,72	20,53	29,66	38,41	44,28
	Drag	2,11	2,51	3,51	4,95	6,51
	L/D	5,08	8,18	8,46	7,76	6,81
Split-tip	Lift	11,62	22,31	32,54	41,27	48,20
	Drag	2,27	2,72	3,84	5,18	7,12
	L/D	5,12	8,21	8,46	7,97	6,77
Split-tip sharklets	Lift	11,16	21,48	31,22	40,73	46,97
	Drag	2,18	2,59	3,62	5,12	6,79
	L/D	5,12	8,30	8,63	7,96	6,92
Blended	Lift	11,50	21,98	31,84	41,27	47,76
	Drag	2,19	2,63	3,66	5,18	6,84
	L/D	5,24	8,36	8,71	7,97	6,98
Fenced	Lift	10,58	20,54	29,77	38,24	45,25
	Drag	2,24	2,61	3,60	4,99	6,65
	L/D	4,72	7,87	8,28	7,67	6,81
Sharklets, upwards	Lift	11,39	22,00	31,99	41,44	48,03
	Drag	2,13	2,57	3,65	5,23	6,89
	L/D	5,35	8,57	8,77	7,93	6,97
Sharklets, downwards	Lift	11,32	21,83	31,70	40,62	47,44
	Drag	2,06	2,50	3,59	5,13	6,91
	L/D	5,49	8,74	8,83	7,91	6,86
Spiroid	Lift	11,02	21,16	30,79	39,76	46,26
	Drag	2,26	2,66	3,71	5,19	6,79
	L/D	4,87	7,94	8,29	7,66	6,81

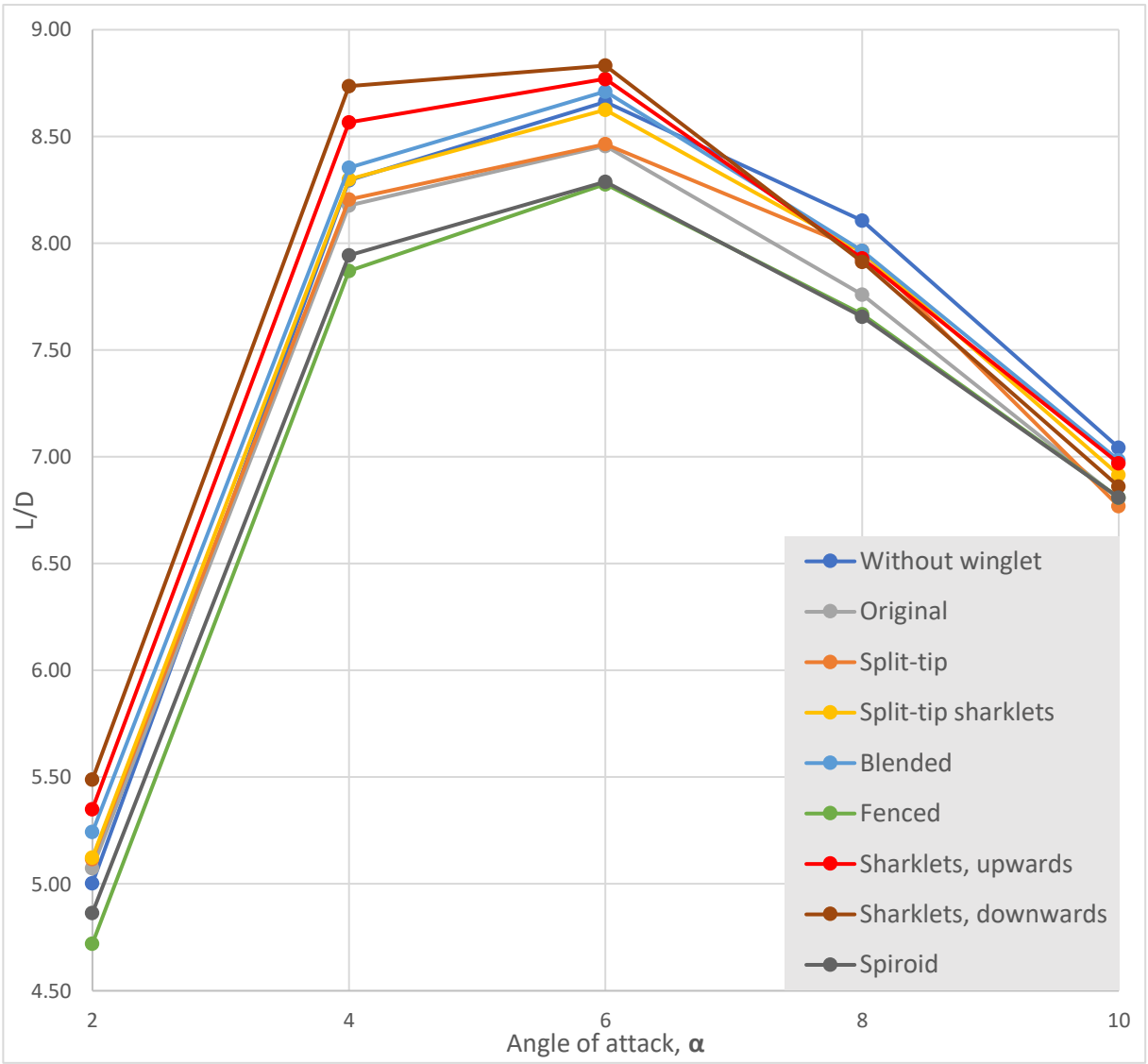

Figure 33: the angle of attack versus the Lift/Drag-ratio evaluated from FloEFD

Discussion

4.1 Limitations and obstacles

Due to limited computational capacity, the range of the datasets were bounded to five angles (α = 2, 4, 6, 8 and 10) with a resolution of two degrees ($\Delta\alpha$ = 2) per observation. And due to the ongoing 2019-20 coronavirus pandemic, no access to KTH's facilities were granted. Therefore, it was not possible to conduct wind tunnel testing for the modelled winglets, which may otherwise have affected the final conclusions drawn from the results.

4.2 Variance in CFD-results

According to the results from both software, one can see that wingtip devices generally provide noticeable improvements over a naked wing at lower angles of attack.

There are however differences in the L/D-ratio between the results from each software, and results obtained from ANSYS Fluent are approximately a factor 1.3 greater than those obtained from FloEFD. Some designs perform better than others according to the two software. For instance, the downward facing sharklet performed better than the upward facing sharklet in FloEFD, which was vice versa in ANSYS Fluent. An explanation could be due to the availability of solver preferences implemented for the respective software. As FloEFD did not provide the equal freedom of solver configurations as ANSYS Fluent, it could be presumed that such settings were not equally configured in both software, which presumably would lead to a variance in the CFD-results.

In general, both software state that the most promising winglets lean towards the sharklets and blended designs, followed closely by the original winglet and split-tip designs. At higher angles, the efficiencies of the wing decrease and the variance of L/D-ratio between the designs drops for both software – the main purpose of wingtip devices is defeated at high angle of attack, according to the calculations. As the angle of attack increases, the flow starts to separate from the trailing edge, leading to decreased performance. As mentioned in the literature review, winglets with lower cant angles are more prone to separation[3], an attribute that possibly could be seen in the results at higher angles of attack. The sharklets, with very low cant angle, have a more noticeable drop in L/D-ratio when the angle of attack increases over 6 degrees. The fenced winglet, with high cant angle, improves compared to the other designs as the angle of attack increases. The blended, also with a higher cant angle than the sharklets, even performed better than these at the highest angles of attack according to the results from both software.

4.3 CFD results versus Literature review

The results from CFD-simulations have also partly differed from the suggestions of the literature review regarding the most efficient designs. According to the literature review, one of the most efficient winglet designs to date is the recently developed split-tip design used in newer Boeing 737 derivatives. This was not the case according to the results from both ANSYS Fluent and FloEFD. Calculations from both software suggested that the sharklet and blended winglets were the most efficient while the split-tip designs underperformed. In the case of ANSYS Fluent, the split-tip models even performed worse than the original winglet under almost all conditions.

When discussing why some winglets underperformed, it is important to bear in mind that specific winglets are designed for specific wings and their flight conditions. A possible explanation to why the results of some designs were falling short if compared to the literature review may be related to the stream velocity which the winglets were subjected to. In the case of this project, the Mach number is no greater than 0,08, which is on par with a conventional highway speed limit for most motor vehicles. At Mach 0,08, the flow is purely subsonic anywhere in the computational domain. Thus, such conditions of flow can be considered incompressible and isochoric, where the laws of thermodynamics can be neglected. In contrast, the free stream velocity of a jetliner at cruising altitude is around 240 m/s (or approximately Mach 0,6-0,9 depending on the cruising altitude), which falls into the spectrum of compressible subsonic flight. At these cruising speeds, the flow is no longer subsonic and incompressible across the wing, where the law of compressible aerodynamics yields. With a far higher cruising velocity, the lift and drag characteristics provided by a winglet may differ from those at low-speed flow conditions, hence resulting in different aerodynamic performances.

In the case of split-tip winglets, Whitcomb stated that the use of a lower winglet in combination with an upper winglet was beneficial at high lift coefficients and supercritical conditions, where the airflow is supersonic over large parts of the cord.[1] At these conditions, winglet designers have to take into account for the formation of supersonic shock waves causing turbulent airflow separation. The lower winglet reduces this separation by reducing the high induced velocities on the forward inner surface of the winglet. It also decreases the velocities at the tip of the wing opposite the forward part of the upper winglet. As the aircraft in this project was tested at Mach 0,08, there was no probability of these phenomena; a possible explanation why the lower winglet in the split-tip designs showed to be more or less otiose.

4.4 Trustworthiness of the CFD results

In general, CFD software packages available today provide in most cases satisfactory results that are comparable to the reality if applied correctly. But there is still much room for improvements according to many aviation experts.[22] Hence, wind tunnel testing still plays a crucial role in aviation research; it is a robust way of verifying results from virtual simulations and will continue to do so for many years to come. However, due to the continuous increasing acceptance of CFD simulations, one can expect CFD software more tightly integrated with physical testing among aviation research and other flow-related studies.

Conclusions

The sharklet designs were most desirable due their high efficiency according to the simulation results. In favor of a more practical and robust aircraft, the upward facing winglets became the winglet of choice for the X8 Skywalker.

The main motive of leaning towards the upward faced design rather than the downward faced one was mainly related to the concern of damaging the winglets during take-offs and landings, due to the elevation difference between the wingtips and the fuselage. Two renders of the X8 Skywalker with the upward faced sharklet winglets are shown in figure 34 and 35.

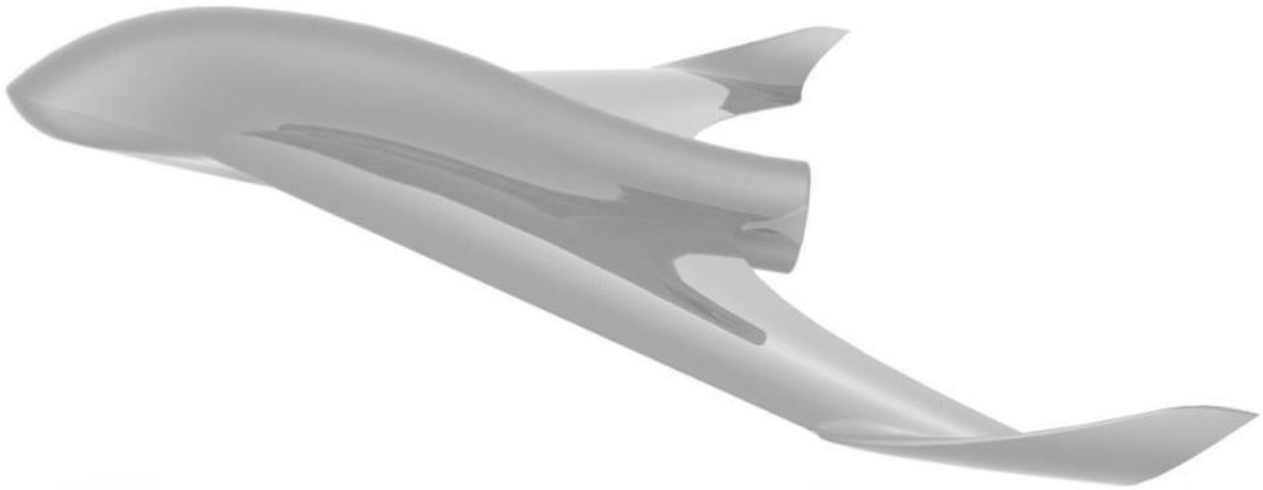

Figure 34

Figure 35

References

1. Richard T. Whitcomb, NACA, 1976, A DESIGN APPROACH AND SELECTED WIND-TUNNEL RESULTS AT HIGH SUBSONIC SPEEDS FOR WING-TIP MOUNTED WINGLETS, https://ntrs.nasa.gov/archive/nasa/casi.ntrs.nasa.gov/19760019075.pdf, July 1976, 2020-04-29

2. Committee on Assessment of Aircraft Winglets for Large Aircraft Fuel Efficiency, 2007, ASSESSMENT OF WINGTIP MODIFICATIONS TO INCREASE THE FUEL EFFICIENCY OF AIR FORCE AIRCRAFT, https://www.nap.edu/read/11839/chapter/5#33, 2007, 2020-05-1

3. Djahid Gueraiche, Sergey Popov, Moscow Aviation Institute, 2017, Winglet Geometry Impact on DLR-F4 Aerodynamics and an Analysis of a Hyperbolic Winglet Concept, https://www.researchgate.net/publication/321846721_Winglet_Geometry_Impact_on_DLR-F4_Aerodynamics_and_an_Analysis_of_a_Hyperbolic_Winglet_Concept, December 2017, 2020-05-11

4. Corporate information - Innovation & technology. Airbus. https://web.archive.org/web/20090421092103/http://www.airbus.com/en/corporate/innovation/, 2009-04-21

5. Nicolas El Haddad, 2015, Aerodynamic and Structural Design of a Winglet for Enhanced Performance of a Business Jet, https://commons.erau.edu/cgi/viewcontent.cgi?article=1264&context=edt, May 2015, 2020-05-11

6. Lauren Penning, Boeing, 2012, Boeing Designs Advanced Technology Winglet for 737 MAX, https://boeing.mediaroom.com/2012-05-02-Boeing-Designs-Advanced-Technology-Winglet-for-737-MAX, 2012-05-02, 2020-04-29

7. Luciano Demasi, Giovanni Monegato, Rauno Cavallaro, Rachel Rybarczyk, 2019, Minimum Induced Drag Conditions for Winglets: the Best Winglet Design Concept, https://www.researchgate.net/publication/330198867_Minimum_Induced_Drag_Conditions_for_Winglets_the_Best_Winglet_Design_Concept, January 2019, 2020-05-11

8. Zabihollah Najafian Ashrafi, Ahmad Sedaghat, 2014, Improving the Aerodynamic Performance of a Wing with Winglet, 2014, https://www.researchgate.net/publication/272175209_Improving_the_Aerodynamic_Performance_of_a_Wing_with_Winglet, November 2014, 2020-05-11

9. William Freitag, E. Terry Schulze, Boeing, 2009, Blended Winglets Improve Performance, https://www.boeing.com/commercial/aeromagazine/articles/qtr_03_09/article_03_1.html, 2009, 2020-04-29

10. Saravanan Rajendran, 2012, Design of Parametric Winglets and Wing tip devices – A Conceptual Design Approach, https://www.diva-portal.org/smash/get/diva2:547954/FULLTEXT01.pdf, 2012, 2020-05-11

11. Sohail R Reddy, Helmut Sobieczky, Abas Abdoli, George S Dulikravich, 2014, Winglets – Multi-Objective Optimization of Aerodynamic Shapes, https://www.researchgate.net/publication/280734280_Winglets_-_Multi-Objective_Optimization_of_Aerodynamic_Shapes, July 2014, 2020-05-11

12. Håkan Abrahamson, Ny Teknik, 2013, Kroksablar på vingarna spar miljard, https://www.nyteknik.se/fordon/kroksablar-pa-vingarna-spar-miljard-6401822, 2013-11-04, 2020-04-29

13. W.Lishifelshyal, 2016, ANALYSIS OF DRAG OVER A WING MODEL WITH & WITHOUT RAKED WINGTIP, https://eprajournals.com/jpanel/upload/706pm_11.W.Lishifelshyal-11.6.16.pdf, June 2016, 2020-05-11

14. Debbie Heathers, Boeing, 2002, New Boeing 777 Raked Wing Tips Improve Fuel Efficiency, Good for the Environment, https://boeing.mediaroom.com/2002-10-01-New-Boeing-777-Raked-Wing-Tips-Improve-Fuel-Efficiency-Good-for-the-Environment, October 2002, 2020-04-29

15. Gautham Narayan, Bibin John, 2016, Effect of winglets induced tip vortex structure on the performance of subsonic wings, https://www.sciencedirect.com/science/article/abs/pii/S1270963816305569, September 2016, 2020-05-11

16. Suhail Mostafa, Shyam Bose, Archana Nair, Mansoor Abdul Raheem, Thasneem Majeed, Atiqur Mohammed, Young Kim, 2014, A parametric investigation of non-circular spiroid winglets, https://www.researchgate.net/publication/262948452_A_parametric_investigation_of_non-circular_spiroid_winglets, 2014, 2020-05-11

17. Ali Murtaza, Dr. Khalid Parvez, Hanzala Shahid, Yasir Mehmood, 2017, DESIGN AND COMPUTATIONAL FLUID DYNAMIC ANALYSIS OF SPIROID WINGLET TO STUDY ITS EFFECTS ON AIRCRAFT PERFORMANCE, https://www.irjet.net/archives/V4/i12/IRJET-V4I12239.pdf, December 2017, 2020-05-11

18. Aviation Partners, Inc. Types of Blended Winglets, https://www.aviationpartners.com/aircraft-winglets/types-blended-winglets/, 2020-04-29

19. M. Chmielewski, M. Gieras, 2013, Three-zonal Wall Function for k-ε Turbulence Models, http://cmst.eu/wp-content/uploads/2013/05/10.12921_cmst.2013.19.02.107-114_Chmielewski.pdf, May 2013, 2020-05-17

20. Simscale, K-epsilon, https://www.simscale.com/docs/content/simulation/model/turbulenceModel/kEpsilon.html, 2020-04-29

21. Shawn Wasserman, Choosing the Right Turbulence Model for Your CFD Simulation, https://www.engineering.com/DesignSoftware/DesignSoftwareArticles/ArticleID13743/Choosing-the-Right-Turbulence-Model-for-Your-CFD-Simulation.aspx, November 2016, 2020-05-27

22. Ben Sampson, The future role of wind tunnels and development, https://www.aerospacetestinginternational.com/features/the-future-role-of-wind-tunnels-in-test-and-development.html, Mars 2018, 2020-05-18